

Impact of FORMOSAT-3/COSMIC radio occultation data on the prediction of super cyclone Gonu (2007): a case study

S. K. A. V. Prasad Rao Anisetty · Ching-Yuang Huang ·
Shu-Ya Chen

Received: 24 July 2013 / Accepted: 20 September 2013 / Published online: 29 September 2013
© Springer Science+Business Media Dordrecht 2013

Abstract This study aims to present an encouraging example of prediction of super cyclone Gonu over the northern Indian Ocean in 2007. A series of experiments are conducted using the advanced Weather Research and Forecasting model with three-dimensional variational method to assimilate GPS RO refractivity from FORMOSAT-3/COSMIC (hereafter referred as GPS) and radiosonde sounding (GTS) to highlight the relative impact of GPS RO data on model prediction. Significant differences in cyclone track and intensity prediction are exhibited in various experiments with and without cyclic assimilations. Both cold-start (non-cyclic) and hot-start (cyclic) runs with GPS RO data exhibit improvement on later track prediction compared to the control run without data assimilation. GPS experiment outperforms other experiments including GTS in track prediction with the smallest cross-track error. Sensitivity tests were also conducted to identify which GPS RO sounding gives more impact on track prediction. We found that the sounding closest to the cyclone exhibits the largest contribution to track prediction. Assimilation of the RO soundings in the vicinity of Gonu cyclone appears to modify the environmental conditions that result in a later development of a couplet of high and low pressure, leading to a positive impact on track prediction. Sensitivity experiments indicate that the initial information retrieved by GPS data at upper levels that produce colder temperature increments indeed contributes more improvement to track prediction.

Keywords GPS radio occultation · COSMIC · WRF model · 3DVAR · Super cyclone Gonu

S. K. A. V. Prasad Rao Anisetty · C.-Y. Huang (✉)
Department of Atmospheric Sciences, National Central University, No. 300, Zhongda Rd., Zhongli City,
Taoyuan County 32001, Taiwan
e-mail: hcy@atm.ncu.edu.tw

S. K. A. V. Prasad Rao Anisetty · C.-Y. Huang
GPS Science and Application Research Center, National Central University, Zhongli City, Taiwan

S.-Y. Chen
University Corporation for Atmospheric Research, Boulder, CO, USA

1 Introduction

Tropical cyclones are the most devastating weather phenomena, and the prediction of tropical cyclones is a challenging issue for weather forecasters. A major problem of tropical cyclone prediction arises due to sparseness of the observations over the oceans. As a result, the initial conditions for a forecast model do not realistically depict the true state of the atmosphere. Initial conditions can be improved by making use of satellite data, e.g., satellite-based rain gauge measurements of rainfall through a physical initialization procedure (e.g., Krishnamurti et al. 1993, 1995). Apart from those data sets, another important source of data is contributed by GPS RO observations. FORMOSAT-3/COSMIC (Constellation Observing Systems for Meteorology, Ionosphere and Climate) is an important international satellite project in this regard to provide global sounding measurement. The complete description and scientific impacts of COSMIC have been given by Anthes et al. (2008). The GPS RO measurement plays a robust role in characterizing planetary atmospheres since the 1960s (Kliore et al. 1964), because it possesses beneficial features of uniform data coverage on the globe, no instrument drifting, high vertical resolution (up to few meters) and little affected by clouds, precipitation and aerosols (Kursinski et al. 2000). GPS-emitted ray can propagate through severe weather systems like heavy rain, cyclones and typhoons without contamination of the signal, whereas microwave radiometers are somewhat affected by clouds and light rain, and infrared (IR) radiometers are contaminated as well by clouds and aerosols (Kursinski et al. 1997). The coverage of radiosondes is rather uneven over the globe and in particular is very poor over the oceans. Furthermore, its temporal resolution is also fairly low (operationally 12-h frequency).

Various model experiments have shown that GPS RO soundings exhibit positive impacts on global and regional weather predictions (Kuo et al. 1997, 2000; Zou et al. 1999, 2000; Liu and Zou 2003; Healy et al. 2005; Healy and Thepaut 2006; Cucurull et al. 2006; Huang et al. 2007, 2010; Healy 2008; Poli et al. 2008, 2010; Cucurull 2010). In particular, typhoon forecasts were improved as well when GPS RO refractivity was assimilated into models (Huang et al. 2005, 2010; Chen et al. 2009; Kueh et al. 2009). We note that the above typhoon case studies have not detailed the processes of individual RO sounding and identify which vertical level is contributing to the improvement of forecasts.

The impact of FORMOSAT-3/COSMIC RO refractivity on the prediction of the super cyclone Gonu (2007) has been briefly introduced in Huang et al. (2010). In this study, we elaborate this case to identify and highlight RO data impacts. We explore the importance of specific GPS RO soundings, the mechanism for the improved track prediction and their contributions from different vertical heights. Analyses of initial changes due to assimilation of GPS RO observations are conducted. The improvement in track prediction has been analyzed and explained in this study. In this context, we have found several important and essential aspects by conducting various sensitivity experiments. We highlight the importance of upper tropospheric temperature information in driving the cyclone track.

The manuscript is organized as follows. The simulated case and experimental design are given in Sect. 2. The simulation results, including initial analyses as well as track and intensity predictions, are discussed in Sect. 3 with verification against observations and global analysis. We provide possible mechanisms of predicted tracks as degraded or improved by the assimilated observations. The impacts of GPS RO data are further highlighted by sensitivity tests in Sect. 4. Finally, conclusions are given in Sect. 5.

2 The case and numerical experiments

2.1 Data sets

FORMOSAT-3/COSMIC (GPS), GTS and NCEP Aviation Model (AVN) global analysis data sets have been used to analyze the cyclone Gonu. The GTS data set from NCAR contains conventional radiosondes and synoptic surface observations. FORMOSAT-3/COSMIC has been able to provide around 2000 RO soundings per day over the globe since launch (Anthes 2011). NCEP-AVN global analysis at $1^\circ \times 1^\circ$ resolution is used to provide initial first guess and boundary conditions for the three-dimensional variational data assimilation (3DVAR) of WRF version 2.2 in this study.

2.2 Cyclone Gonu

Gonu was the first-ever super cyclone formed over the Arabian Sea and was the strongest tropical cyclone on record in the Arabian Sea. This motivates the authors to choose this cyclone Gonu. Intense cyclones, like Gonu, are rare over the Arabian Sea, and most of the storms in this area tend to be small and dissipate quickly. The Indian monsoon flow was disrupted due to the formation of the super cyclone Gonu. A widespread area of convection was observed over the southeastern Arabian Sea on May 27, 2007 and then an organized tropical disturbance with a mid-level circulation developed at about 645 km off the coast, south of Mumbai, India, on 31 May. Late on 1 June, the system was classified as a depression by India Meteorological Department (IMD), and then it reached to a severe cyclonic storm by 3 June. The cyclone reached the maximum wind speed of 268 km h^{-1} (~ 145 knots) and the minimum sea-level pressure of 914 hPa by 1200 UTC 4 June; IMD classified the cyclone as super cyclone Gonu at this stage. After 6 h (i.e., 1800 UTC 4 June), the sea-level pressure deepened to 898 hPa. By 5 June, the cyclone weakened to a severe cyclonic storm. The eye of the cyclone became cloudy; the cyclone gradually weakened due to cooler sea-surface water temperature and dry air as it intruded the Arabian Peninsula. Because of interaction with land at Oman, the inner core of deep convection weakened rapidly, and the flow intensity decreased at a rate of 95 km h^{-1} ($\sim 26 \text{ m s}^{-1}$). According to the IMD, cyclone Gonu crossed the eastern tip of Oman with the maximum wind of 150 km h^{-1} late on 5 June. After emerging into the Gulf of Oman, the cyclone re-intensified slightly. However, increasing wind shear and entrainment of the dry air from the Arabian Peninsula continued to suppress deep convection from its eastern semicircle. On 6 June, the cyclone turned to the north–northwest, and later the joint typhoon warning center (JTWC) downgraded Gonu to tropical storm category. Gonu crossed the Oman coast and subsequently the Makaran coast on 7 June. According to news reports, cyclone Gonu caused severe damages and a variety of losses throughout Oman and south Iran (worth \$4 billion and \$216 million US, respectively).

2.3 Experimental design

The numerical experiments conducted in this study use the Weather Research and Forecasting (WRF 2.2) model with 3DVAR (Barker et al. 2004) to assimilate various data sets like GPS RO and GTS soundings, and their combination. The horizontal resolutions of the model are 45 and 15 km for domain 1 (larger) and domain 2 (smaller), respectively, as shown in Fig. 1. Since the focus of this study is on track prediction, use of a horizontal

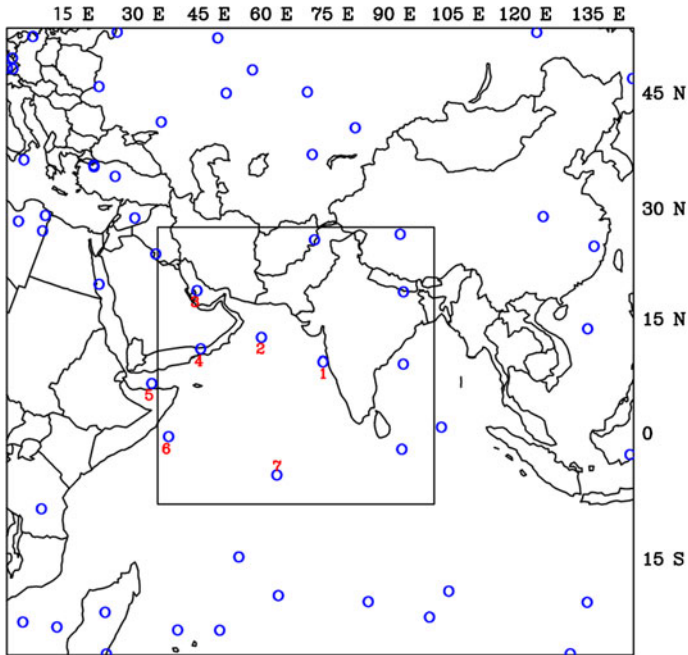


Fig. 1 Two nested domains with horizontal resolutions of 45 (domain 1) and 15 km (domain 2), respectively. Geographical distributions of assimilated FORMOSAT-3/COSMIC RO soundings are illustrated in domain 1. Circle (blue) indicates the location of RO sounding, and the number (red) denotes the removed sounding for sensitivity test

resolution of 15 km for the inner domain should be reasonable. The model has a vertical resolution of 28 layers with stretched grids and a top height at 50 hPa. For cold start, the model is integrated for 96 h starting from the initial time at 0000 UTC June 3, 2007, with the Goddard cloud microphysics, Kain-Fritsch cumulus parameterization and YSU PBL parameterization employed in both domains. These schemes are extensively used for tropical cyclone prediction over Bay of Bengal and west Pacific Ocean (Raju et al. 2011; Potty et al. 2012). The initial first guess and boundary conditions are taken from NCEP-AVN global analysis, and the NCEP background error covariance (B) used in the 3DVAR data assimilation.

A series of numerical experiments were conducted to investigate cyclone Gonu with assimilation of different combinations of the data sets (see Table 1). The 3DVAR was performed only for the coarse domain to assimilate the observations within 3 h of the model initial time, i.e., from 2100 UTC June 2 to 0003 UTC June 3, 2007 (the assimilation window). The model analysis in the fine domain is interpolated from the coarse domain. A total of 56 GPS RO soundings available from FORMOSAT-3/COSMIC were observed in the coarse domain as shown in Fig. 1. Circle (blue) indicates the location of RO sounding, and the number (red) denotes the removed sounding for sensitivity test. Apart from the aforementioned simulations, a series of sensitivity experiments were performed by removing some of the GPS RO soundings around the cyclone to identify the relative impacts of these soundings. The control run (CTL) was conducted without assimilation of any observations. Also, cyclic experiments with a 6-h assimilation window were held using GPS (hereafter refer as GPS-cyc) and GTS (hereafter refer as GTS-cyc) with initial time

Table 1 Summary of model experiments

Exp. no	Name of the experiment	Description of the experiment
1	CTL	Control run without data assimilation
2	GPS	GPS RO refractivity data from FORMOSAT-3/COSMIC
3	GTS	GTS radiosondes
4	GPS + GTS	Combination of GPS and GTS
5	GPS-cyc	GPS cyclic assimilation of 12 h (with every 6 h + 6 h)
6	GTS-cyc	GTS cyclic assimilation of 12 h (with every 6 h + 6 h)

from 2 June 12 UTC to 3 June 00 UTC (12-h cyclic). A total of 234 GPS RO soundings are found in an assimilated domain for GPS-cyc. For these hot-start cyclic runs, the model forecast at the assimilation time is used as the background in the 3DVAR.

There are two kinds of refractivity operators in WRF 3DVAR to assimilate the GPS RO soundings, i.e., local and non-local refractivity operators. In brief, a local refractivity operator assimilates the RO retrieved refractivity as a local point measurement (Huang et al. 2005), whereas a non-local refractivity operator assimilates the integrated refractivity along a straight ray path (Liu et al. 2008; Ma et al. 2009). The non-local refractivity operator implemented in WRF 3DVAR (Chen et al. 2009) was used for this case study. The non-local refractivity operator is briefly described below.

The neutral atmospheric refractivity N is given by

$$N = 77.6 \frac{P}{T} + 3.73 \times 10^5 \frac{P_w}{T^2}, \quad (1)$$

where P is the pressure of the atmosphere in hPa, T is air temperature in K, and P_w is water vapor pressure in hPa. To account for non-local effects, the model local refractivity needs to be integrated along a ray path that is approximated by a straight line (Sokolovskiy et al. 2005a, b). This line integral is treated as a new observable (excess phase), defined as $S = \int N dl$, where l is the raypath in the model domain. This non-local effect may reduce the representative errors caused by horizontal gradients. More details about the non-local operator and associated observational errors can be found in Chen et al. (2009, 2011).

3 The simulation results

3.1 Analyses of initial increments

Figure 2 shows the increments of moisture and temperature for GPS and GTS at the model initial time of 0000 UTC June 3, 2007. The increments are the differences between the analysis results (after the assimilation of the observations) and the background (as the first guess) in the 3DVAR. Note that negative (positive) increments, i.e., negative (positive) contours in the figure, indicate that the initial background is too moist (dry) for water vapor and too warm (cold) for temperature, compared to the observations. The maximum (minimum) values of moisture increment for GPS and GTS at the level of 836 hPa are 0.8 (−2.2) and 2.8 (−3.2) g kg^{−1}, respectively. GPS assimilation produces drier water vapor, especially over the south Indian Ocean (Fig. 2a), which is even less in magnitude than with GTS assimilations. The maximum (minimum) temperature increments for GPS and GTS

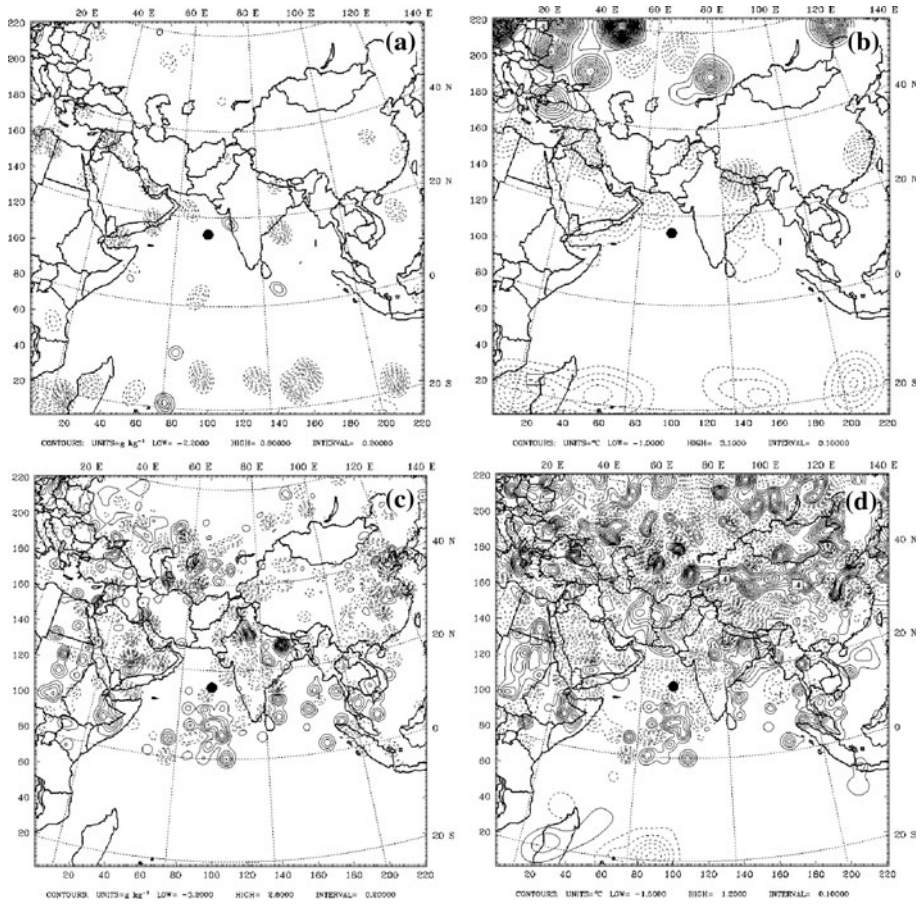


Fig. 2 The initial increments of **a** water vapor mixing ratio (at an interval of 0.2 g kg^{-1}), **b** temperature (at an interval of $0.1 \text{ } ^\circ\text{C}$) for GPS RO at model sigma level of 0.81 (836 hPa), **c** and **d** same as **a** and **b**, respectively, but for GTS. The *black dot* in each panel represents the center of super cyclone Gonu

are 3.1 (-1.0) and 1.2 (-1.5) $^\circ\text{C}$, respectively. As expected, assimilation with various GTS soundings leads to widespread modifications mostly over the land. There are higher values of temperature increment at the north boundary of the outermost domain when GPS RO soundings are assimilated. This might indicate a large departure of the RO refractivity from the background refractivity as the moisture becomes drier at higher latitudes. On the other hand, the analysis temperature is colder over the south Indian Ocean, upstream of Gonu cyclone, in association with the drier moisture.

To further understand moisture increments, we plot north–south vertical cross-section for GPS RO soundings around the cyclone as shown in Fig. 3. The GPS RO sounding 1 (Fig. 3b) located near the west coast of India shows positive increments between 0.5 and 5.5 km heights, and the sounding 6 (Fig. 3e) near Somalia coast also shows positive increments from 1 to 8 km height, while rest of the GPS RO soundings around the cyclone give negative increments at all the heights except for the GPS RO sounding 7 (Fig. 3c) with smaller positive increments above 7 km height. The east–west (figures not shown) vertical cross-section is similar to north–south vertical cross-section. The lateral extent of

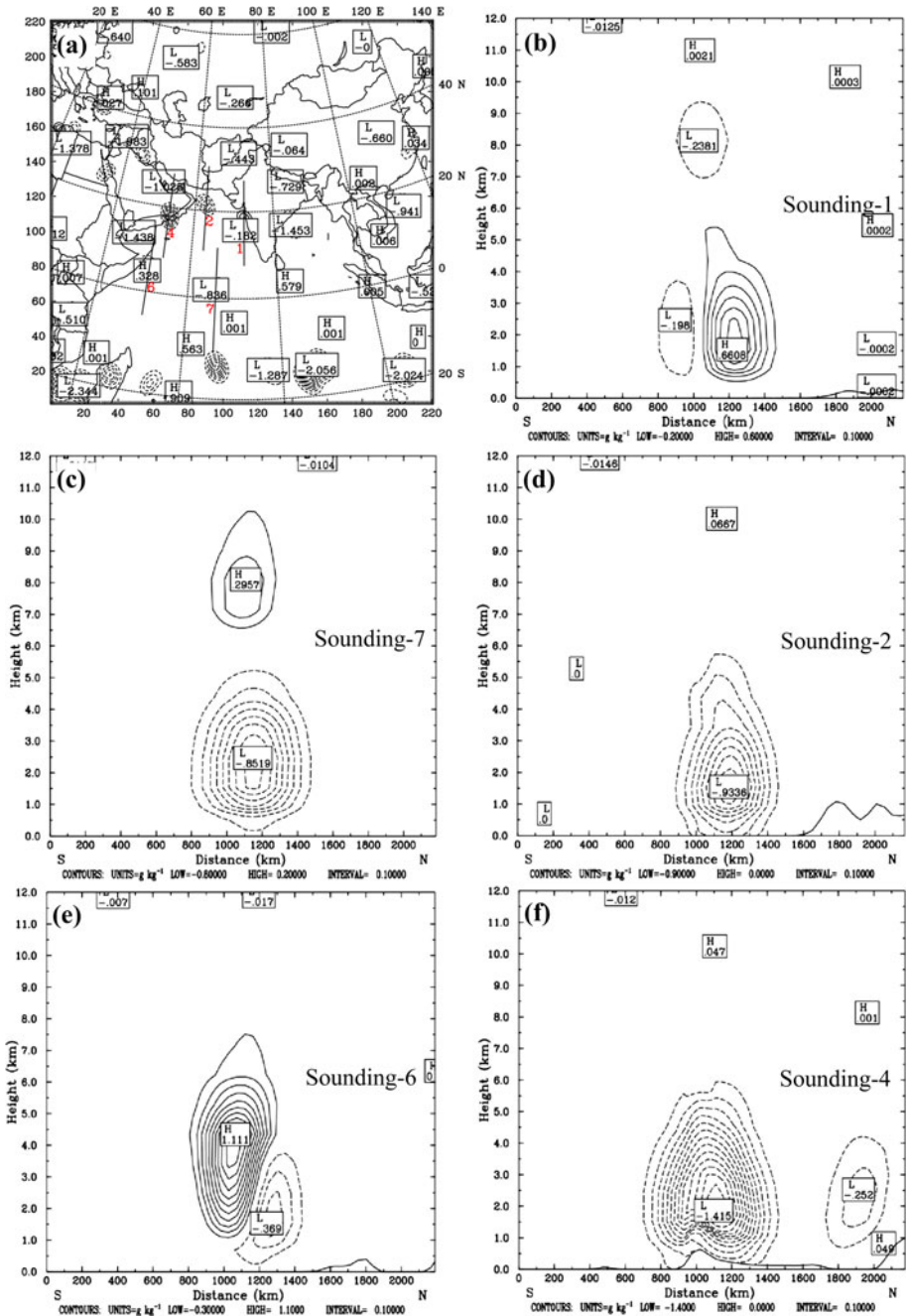


Fig. 3 North–south cross-section of moisture increment (at an interval of 0.1 g kg^{-1}) at the model initial time 0000 UTC June 3, 2007

the main increment is about 600 km since the path of a ray that propagates within the model domain is less than 1,000 km (Zou et al. 1999).

Figure 4 shows the vertical profiles of moisture increments (g kg^{-1}) as well as temperature increments ($^{\circ}\text{C}$) from 0 to 20 km height for GPS RO soundings around the cyclone Gonu. The GPS RO sounding 1 (Fig. 4a) near the west coast of India produces positive moisture increments with the highest magnitude of 0.5 g kg^{-1} ; the

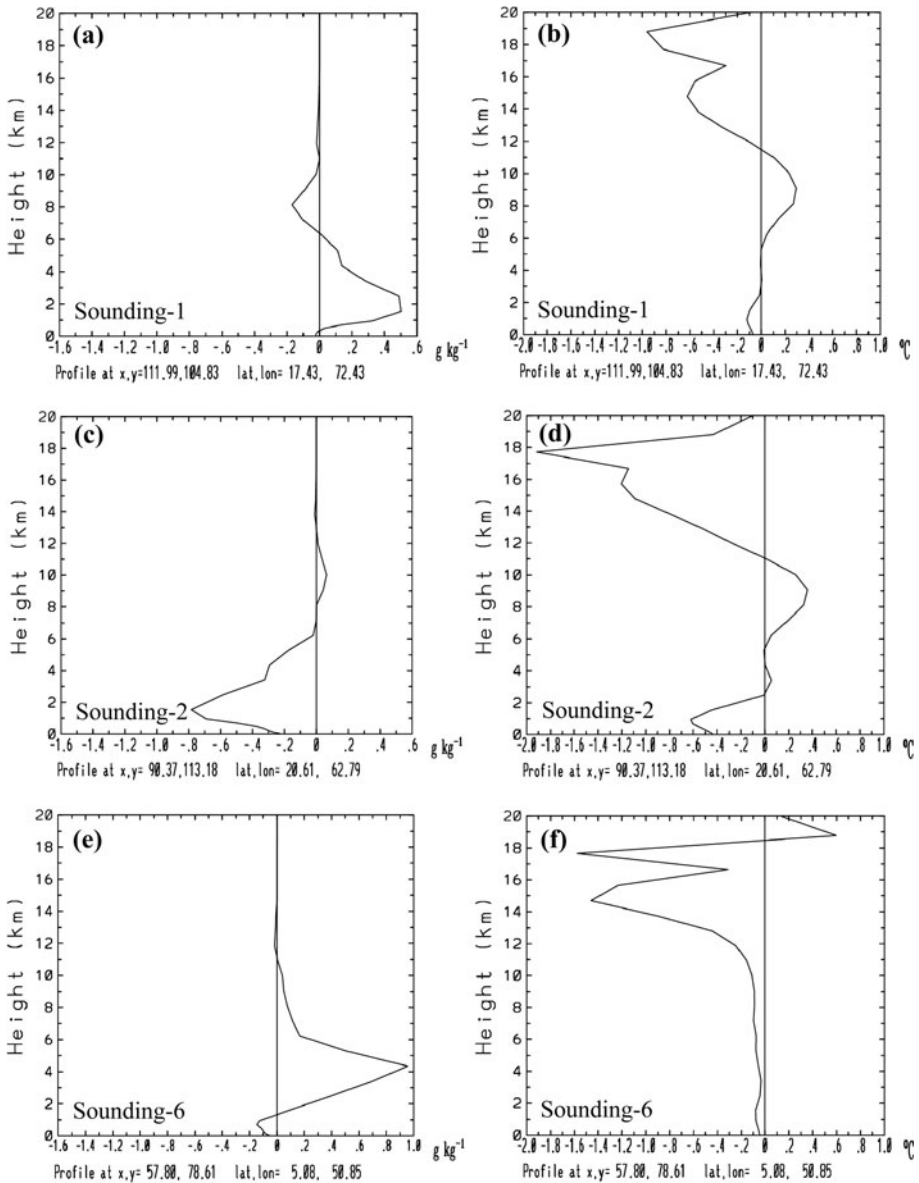


Fig. 4 Vertical initial increments for various RO soundings. **a**, **c** and **e** are for moisture increments (g kg^{-1}), and **b**, **d** and **f** are for temperature increments ($^{\circ}\text{C}$)

corresponding temperature increments (Fig. 4b) are rather small. The GPS RO sounding 6 (Fig. 4e), near the Somalia coast, shows positive moisture increments similar to those for the sounding near the west coast of India. The GPS RO sounding 2, located north of the cyclone center (Fig. 4c), shows negative moisture increments from the surface to 6 km. Temperature increments at lower levels are not as large as at higher levels where significant cooling exists (up to -2 °C) and tends to affect the cyclone track as shown later in sensitivity tests. It appears that assimilation of the GPS RO refractivity contributes mainly to moisture increments at lower levels but to temperature at upper levels where much less water vapor amounts normally exist.

The initial wind speed increments for GPS and GTS are shown in Fig. 5. For east–west wind component, GPS shows negative increments associated with an anti-cyclonic circulation near the Somalia coast on Indian Ocean (Fig. 5a), and it could be the cause to slow down the track (shown later) predicted by GPS run. GTS shows anti-cyclonic shear over the north Arabian Sea (Fig. 5b) south of which cyclonic shear exists over north Indian Ocean above the equator. Consequently, it enhances the movement of the cyclone. All the simulated tracks will be shown in Sect. 3.3.

3.2 Verification of the model results

The results of CTL and GPS are verified (Fig. 6) by the root mean square error (RMSE) of the model analysis and prediction against global analysis. The forecast results of GPS and CTL are compared with NCEP-AVN and ECMWF global analyses for every 6 h of the model forecast time in the target part of domain 1 (the domain area is similar to domain 2 in Fig. 1). Verification against global analysis may not fully indicate the true state in this study. However, both NCEP-AVN and ECMWF global analyses have assimilated available observations and may provide the realistic environmental condition of large scale.

The induced biases are larger for whole domain 1 due to high mountains of Tibetan plateau and the contrast between the land and the ocean. Therefore, we choose some part of domain 1 which is similar to domain 2, and the validation has been chosen to compare root mean square error (RMSE) of wind components (U and V) (m s^{-1}), temperature (°C), mixing ratio (g kg^{-1}), pressure (hPa) and refractivity (N-units). The RMSEs in general are similar when compared with ECMWF and NCEP analyses. Note that at the initial time, the difference between NCEP and CTL is identical to zero since the initial condition of CTL uses the NCEP global analysis. The difference following the time between ECMWF and GPS is larger than that between NCEP and GPS, because the initial condition of GPS also uses NCEP global analysis except with assimilation of the GPS RO data. The errors of U-component (Fig. 6a) are slightly larger for GPS as compared to CTL in the entire simulation period. The errors of V-component for GPS (Fig. 6b) are reduced from 48 to 96 h, so northerlies are more dominant to make the GPS track closer to the best track at the later stage of simulation. Moisture errors (Fig. 6d) for GPS are larger up to 66 h but become smaller from 72 to 96 h. The temperature errors are smaller for GPS at the later stage. The pressure errors (Fig. 6e) against both NCEP and ECMWF analyses for GPS are larger till 24 h but become smaller from 42 h to the end of simulation as compared to CTL. The refractivity errors (Fig. 6f) are reduced as well for GPS at the later stage, in consistency with moisture errors.

3.3 Cyclone track and intensity prediction

Figure 7 shows the best track and the simulated tracks for 96 h. The simulated tracks are much less uniform till 24 h of integration. The track is determined by the center with a

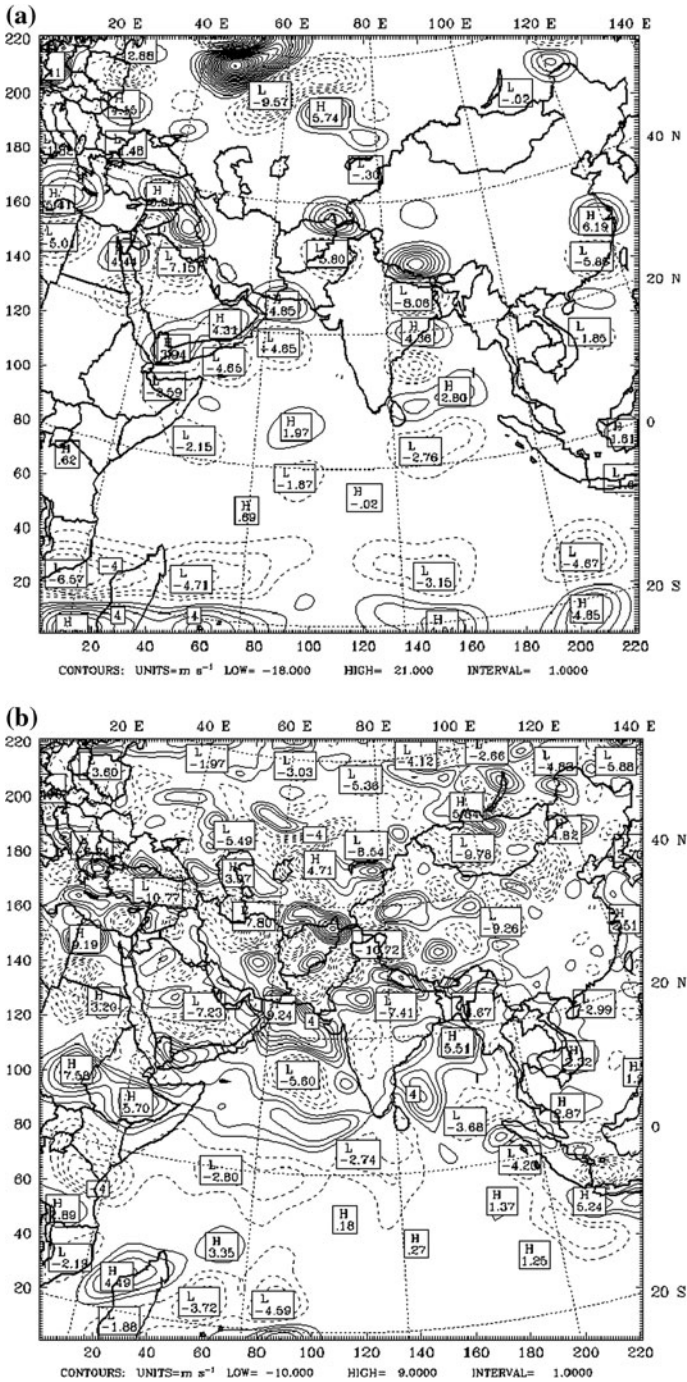


Fig. 5 The initial increments of horizontal wind speed (an interval of 1 m s^{-1}) in x-direction for domain 1, at sigma level of 0.81 (836 hPa) after assimilation of **a** GPS RO data, **b** GTS data

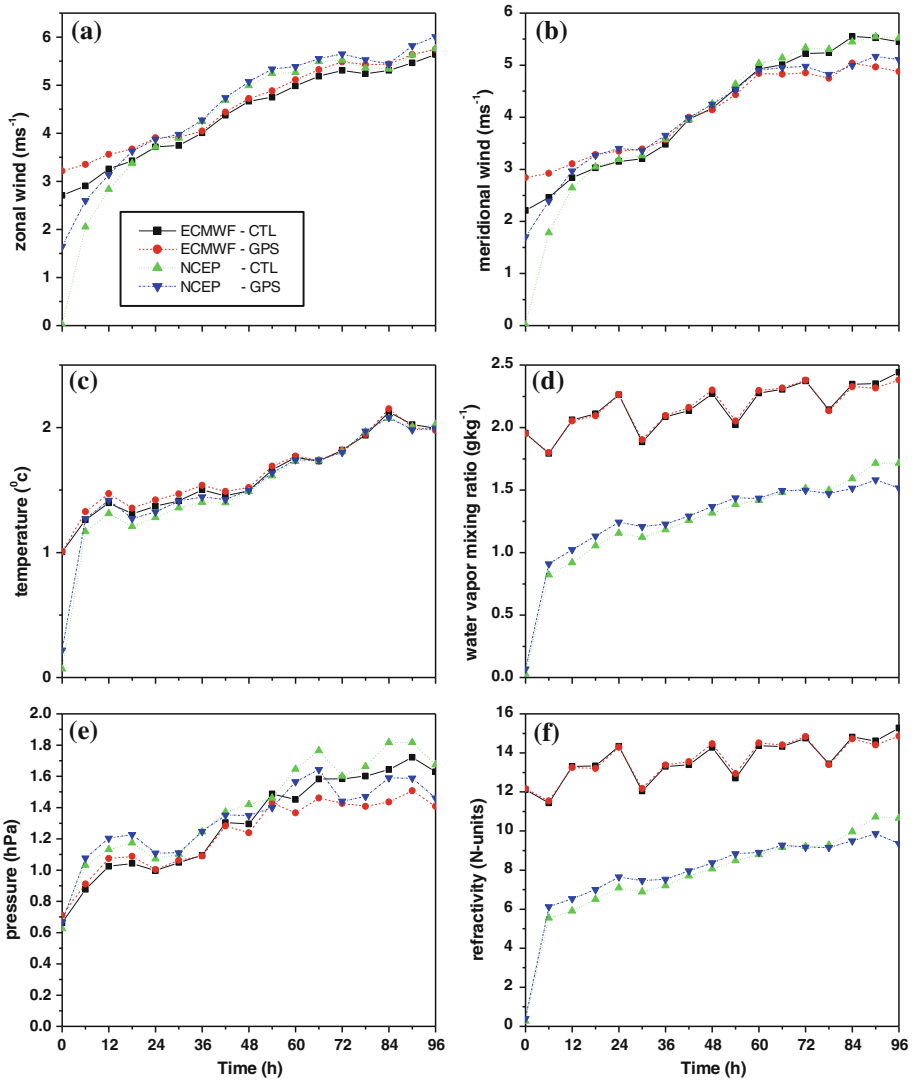


Fig. 6 Time evolution of root mean square error (RMSE) in some part of domain 1 (similar to domain 2). **a** Zonal wind ($m s^{-1}$), **b** meridional wind ($m s^{-1}$), **c** temperature ($^{\circ}C$), **d** mixing ratio ($g kg^{-1}$), **e** pressure (hPa) and **f** refractivity (N-units). RMSE is the model verification against ECMWF and NCEP global analyses

minimum sea-level pressure that in fact jumps irregularly at the incipient stage as the cyclone has not intensified. Hence, the comparisons of the simulated tracks will be focused on later stages. The CTL gives a track close to the best track from 24 to 72 h, but later the track exhibits an eastward tendency. Assimilation of GPS RO refractivity soundings helps improve the track in closest approximation to the best track from 24 to 60 h, and then with a slightly westward deviation till 72 h and again sticks to the best track from 72 to 96 h. With more assimilated RO data, GPS-cyc outperforms all the other simulations till day 3. Numerous sensitivity experiments focusing on cold start are conducted by removing some

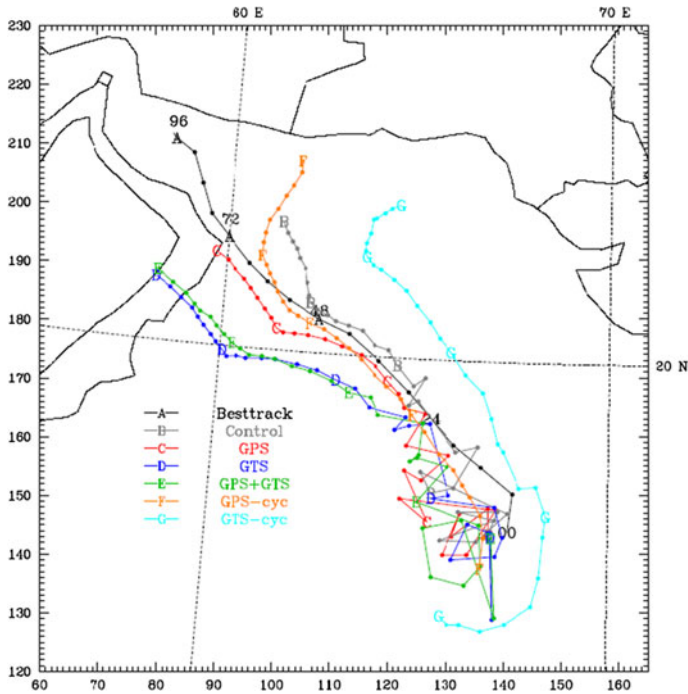


Fig. 7 Tracks of the cyclone Gonu in domain 2 for 96 h starting at 0000 UTC June 3 and ending at 0000 UTC June 7, 2007, for the JTWC best track A, Control B, GPS C, GTS D, GPS + GTS E, GPS-cyc F and GTS-cyc G

GPS RO soundings around the cyclone to identify which sounding plays a more dominant role in track prediction, and those results are presented in Sect. 4.

The assimilation of GTS and the combination of these two data sets show comparable tracks from 24 to 60 h, but later all these tracks deviate westward from the best track. All the assimilation experiments show better agreement with the observations on days 2 and 3 compared to day 4, but only GPS produces the track in best agreement with the best track on day 4. Compared to CTL, the track error for GPS is slightly larger on day 1, similar for day 2, but significantly reduced on days 3 and 4. Compared to GTS, the combination of GTS and GPS has shown slightly better performance in track prediction, which infers the benefit of GPS RO soundings. The cyclic run GTS-cyc does not improve the track prediction. For GTS data impact, the hot start seems to incur larger model errors than cold start at the CTL initial time. Nevertheless, the positive impacts of GPS RO data have been presented in both hot-start and cold-start runs.

In summary, the mean track errors for all the experiments are shown in Fig. 8a. GTS-cyc shows largest track errors for the entire simulation period of 96 h. GPS-cyc shows smallest track error for day 1, 2 and 3. GPS shows the larger track error only on day 1, but later the error significantly declines from day 2 to 4 in consistency with the reduced RMSEs of U and V. Both GPS and CTL have comparable track errors in days 2–4, but the cross-track errors for GPS are much smaller in day 4. For GPS + GTS, the track errors in days 1–4 are significantly reduced as compared to GTS.

The simulated minimum SLP at the cyclone center for every 6 h is shown in Fig. 8b. The observed minimum SLP at the model initial time is 978 hPa (0000 UTC 3 June) and

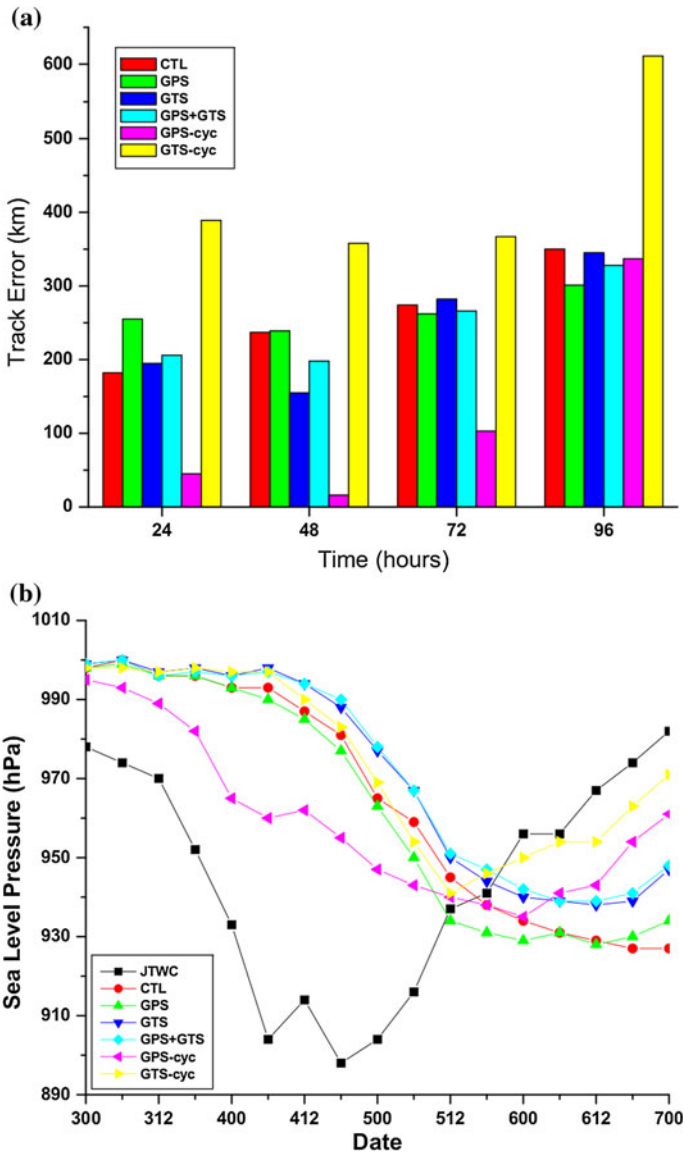


Fig. 8 **a** Time evolution of simulated track errors (km) for CTL, GPS, GTS, GPS + GTS, GPS-cyc and GTS-cyc, and **b** minimum SLPs (hPa) for JTWC best track, CTL, GPS, GTS, GPS + GTS, GPS-cyc and GTS-cyc

then drops drastically until 30 h (0600 UTC 4 June). Later, the SLP slightly increases for 6 h but then deepens to 898 hPa at 1800 UTC 4 June, and then increases gradually to 982 hPa at 0000 UTC 7 June. None of the SLPs for the assimilation runs deepens to the observed. All the assimilation runs show the storm intensity of about 998 hPa at the model initial time, which is about 20 hPa higher than the observed SLP. This is because there is no bogus vortex inserted in the model initial conditions. We avoid vortex bogussing in this

study to simplify the problem of demonstrating observation impact. GPS-cyc remarkably improves the storm intensity within 60 h compared to all other simulations. Compared to CTL, GPS also slightly improves storm intensity till 60 h. However, GPS + GTS is close to GTS till the end of integration. GTS-cyc catches weakening of the storm in day 4.

3.4 Possible mechanisms of predicted tracks

To understand the improvement of GPS track at a later stage (72–96 h), we checked the difference of moisture and SLP between GPS and CTL for domain 2 at model level of 730 hPa as shown in Fig. 9. It is noticed that a couplet of high and low pressure is induced with low (moisture) to the left and high (drier) pressure to the right. This couplet pattern became stronger from 48 h (Fig. 9a) to 60 h (Fig. 9b). The horizontal pressure gradient force might be the reason for why the GPS track is closer to the best track at the later stage. The same couplet pattern is also noticed in the differences of GTS with CTL. Deviation of GTS tracks after 60 h can be attributed to the fact that their couplets are stronger compared to GPS as shown in Fig. 10. Similar to GPS, the low (high) pressure is accompanied by positive (negative) moisture increments for GTS.

4 Forecast sensitivity to GPS RO data

To understand more about which GPS RO sounding plays a more dominant role in the track prediction, a total of nine sensitivity experiments (Table 2) were performed by removing (removed soundings shown in Fig. 1) some of the GPS RO refractivity soundings near the cyclone. Figure 11 shows the simulated tracks for the RO sensitivity tests. The sensitivity test 1 (without the RO soundings 1, 2, 5 and 7) and test 5 (without the RO sounding 2) exhibit that their tracks move northeastward away from the best track, whereas the track for test 5 is even farther away. For test 2 (without the RO soundings 1, 2, 4, 5 and 7), the track is similar to the best track until day 3 and then moves rightward from the best track. Test 3 (without the RO sounding 4), test 4 (without the RO sounding 1) and test 6 (without the RO sounding 5) show that the tracks move southwestward away from the best track. Test 7 (without the RO sounding 7) track overlaps with the best track. Tracks of test 8 (without the RO sounding 3) and GPS experiment (with all the RO soundings) are close to each other. Sensitivity test 9 (without the RO sounding 6) track is close to the best track until 75 h and then overlaps with the best track till the end of the forecast. The above sensitivity tests indicate that the track prediction is most sensitive to removal of the RO sounding 2 (closer to the cyclone center), while all the other soundings at some distance around the center of cyclone Gonu still have some influence, although not as much.

To explore the relative importance of RO observation information at different heights, we conducted several sensitivity experiments (see Table 3) by removing GPS RO soundings at different heights (e.g., down to 3, 5, 8, 10, 12 and 14 km). As shown in Fig. 12, the simulated tracks are less affected when RO soundings below 3, 5, 8, 10 and 12 km are removed. The simulated track deviates much more from the best track when only the sounding information above 14 km is retained. This is because RO-derived dry temperature is accurate at the upper troposphere and hence helps in simulating the upper environmental flow of the cyclone.

To further understand how the tracks are varied by the retained different sounding information, we examine the 730-hPa temperature and SLP differences at 48 and 60 h for domain 2 between the two GPS runs, one with RO soundings above 12 km and the other

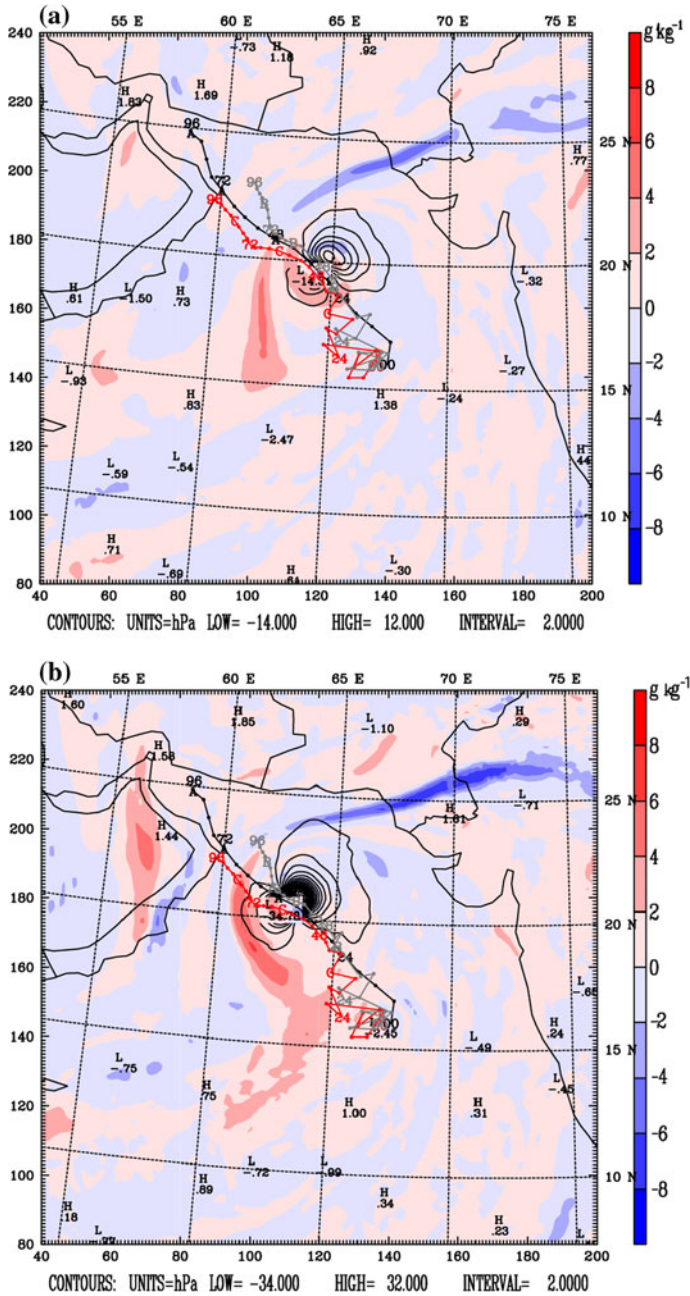


Fig. 9 The difference of moisture and sea-level pressure between GPS and CTL experiments for domain 2 at model level 730 hPa at **a** 48 h and **b** 60 h. Simulated tracks of GPS (C) and CTL (B) are plotted along with the best track (A) for the entire period of simulation

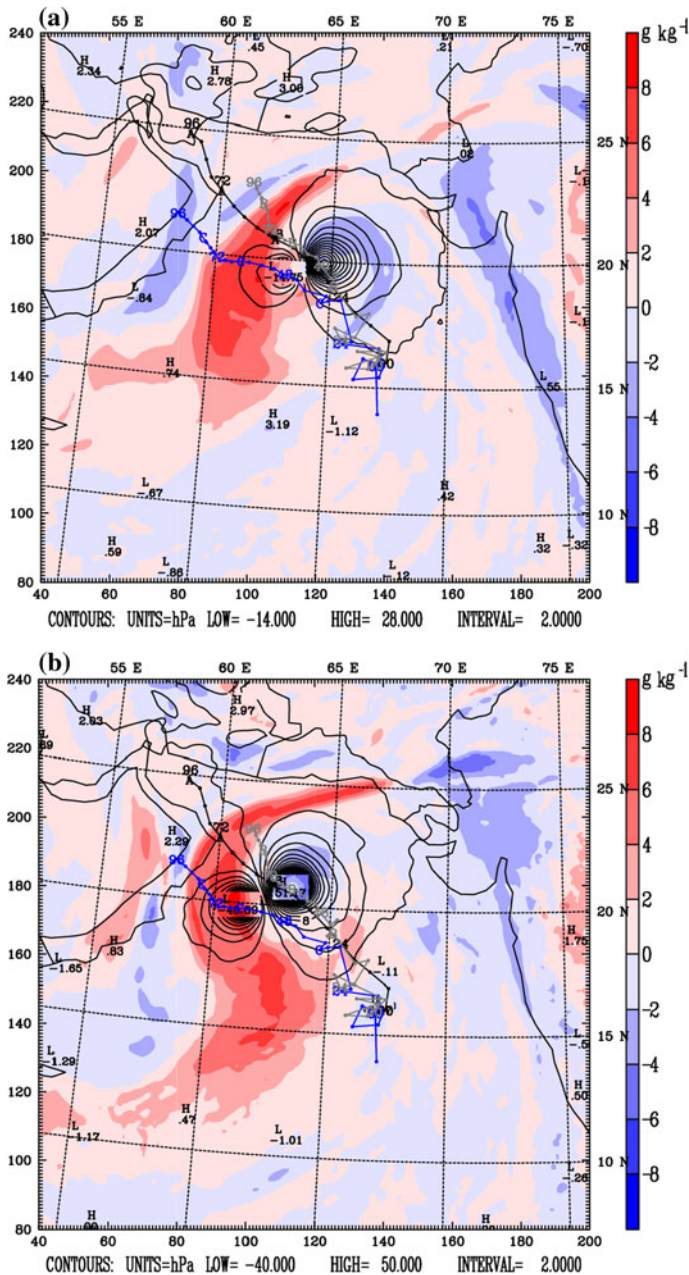


Fig. 10 The difference of moisture at model level 730 hPa and sea-level pressure between GTS and CTL experiments for domain 2 at **a** 48 h and **b** 60 h. **a** and **b** have the simulated tracks of GTS (C) and CTL (B) along with the best track (A) for the entire period of simulation

above 14 km. A couplet with drier temperature to the right of the track and moist temperatures to the left (Fig. 13a, b) is observed. The moist temperature to the left makes the former track closer to the best track. The sea-level pressure pattern (Fig. 13c, d) also shows

Table 2 GPS Sensitivity experiments

Exp. no	Name of the experiment	Description of the experiment
1	GPS sensitivity test 1	Removed RO soundings 1, 2, 5 and 7
2	GPS sensitivity test 2	Removed RO soundings 1, 2, 4, 5 and 7
3	GPS sensitivity test 3	Removed RO sounding 4
4	GPS sensitivity test 4	Removed RO sounding 1
5	GPS sensitivity test 5	Removed RO sounding 2
6	GPS sensitivity test 6	Removed RO sounding 5
7	GPS sensitivity test 7	Removed RO sounding 7
8	GPS sensitivity test 8	Removed RO sounding 3
9	GPS sensitivity test 9	Removed RO sounding 6

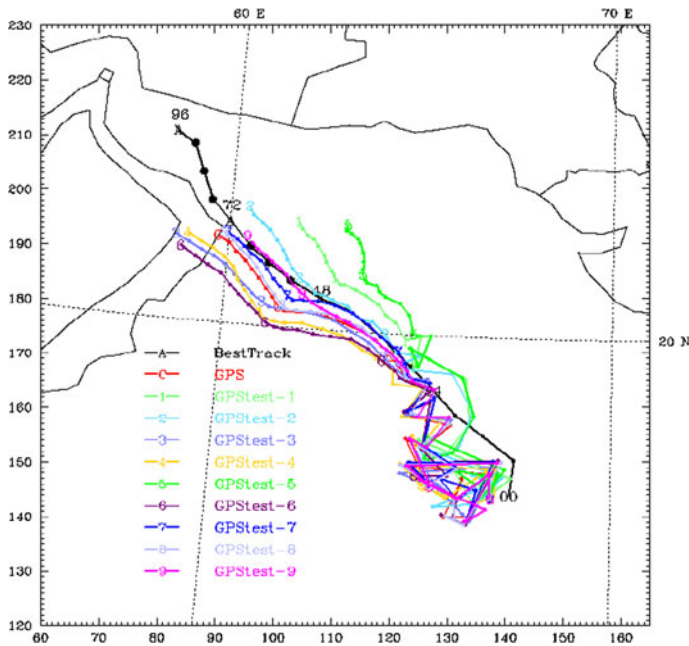


Fig. 11 The simulated tracks of the cyclone Gonu for 96 h for GPS sensitivity experiments (tests 1 to 9) denoted by 1–9, respectively. The best track is denoted by A, and the GPS track with all RO soundings is denoted by C

a couplet with low to the left and high to the right, providing a possible mechanism driving the cyclone toward the best track.

5 Conclusions

In this study, we employ the WRF version 2.2 model to simulate the super cyclone Gonu (2007) over the northern Indian Ocean. To improve the model initial conditions, the three-

Table 3 GPS sensitivity experiments for various heights

Exp. no	Name of the experiment	Description of the experiment
1	GPS above 3 km	GPS RO soundings retained above 3 km
2	GPS above 5 km	GPS RO soundings retained above 5 km
3	GPS above 8 km	GPS RO soundings retained above 8 km
4	GPS above 10 km	GPS RO soundings retained above 10 km
5	GPS above 12 km	GPS RO soundings retained above 12 km
6	GPS above 14 km	GPS RO soundings retained above 14 km

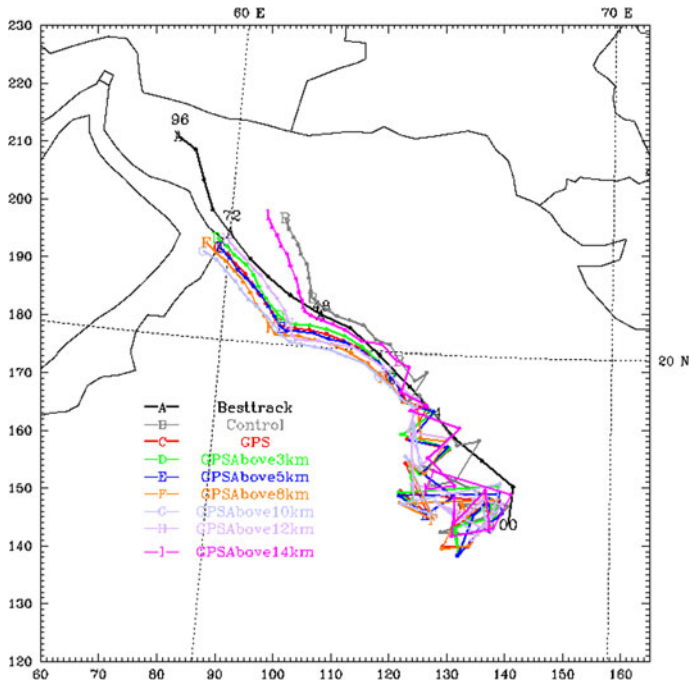


Fig. 12 The tracks of the cyclone Gonu for 96 h for GPS sensitivity experiments, which retain RO soundings above different heights for the best track (A), CTL (without RO soundings) (B) and the experiments with all RO soundings above the surface (C) and above 3 km (D), 5 km (E), 8 km (F), 10 km (G), 12 km (H) and 14 km (I)

dimensional variational (3DVAR) data assimilation system has been used to assimilate different data sets including GPS RO refractivity soundings, GTS and their combination. A non-local refractivity operator (Chen et al. 2009) is applied to assimilate the GPS RO refractivity soundings available from FORMOSAT-3/COSMIC. Based on the model results, GPS RO refractivity soundings exhibit a remarkable positive impact on Gonu's track prediction and outperform the others in terms of the cross-track error at later stages. The impacts have been investigated in detail in this study with regard to contributions from specific RO soundings and observational information above various heights.

Most of the initial moisture increments from the GPS RO soundings laid in a horizontal range of 500–700 km in the lower troposphere, exhibiting drier conditions near the center

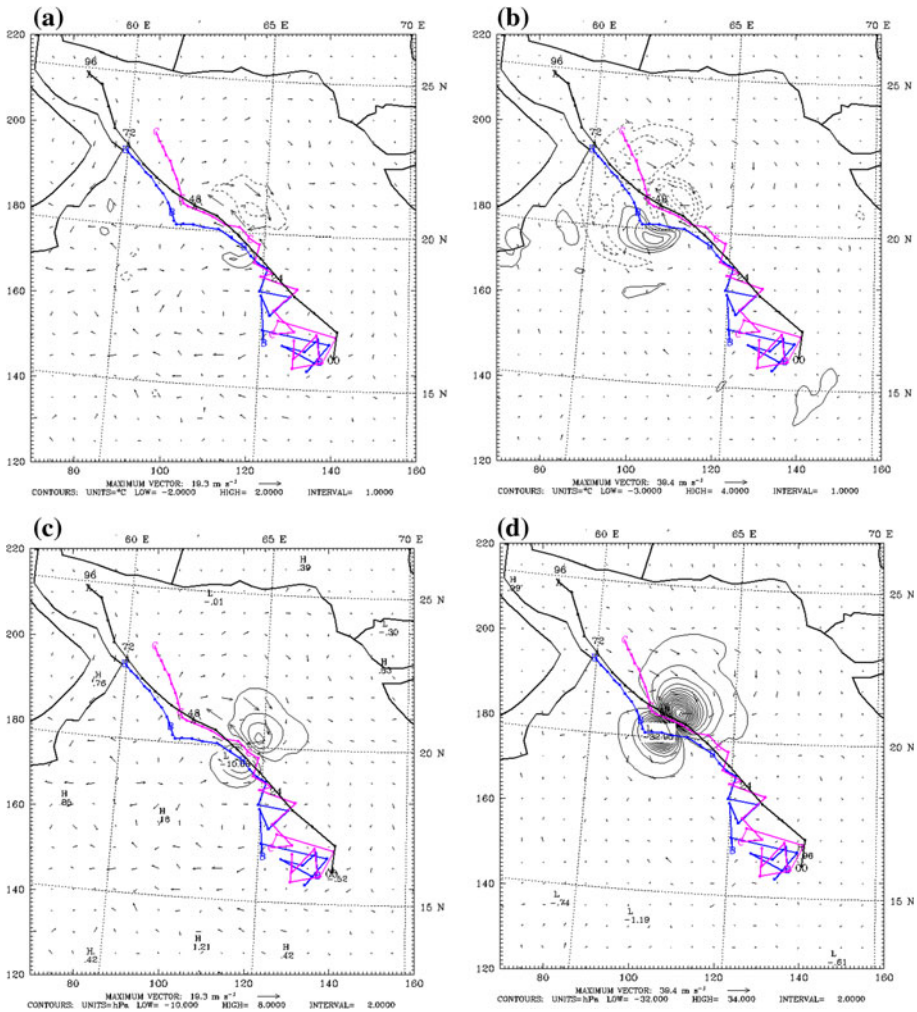


Fig. 13 The differences in temperature between two GPS runs (with RO soundings above 12 and 14 km, respectively) at 730 hPa for domain 2 at **a** 48 h, **b** 60 h, **c** and **d** same as **a** and **b** but for sea-level pressure with their corresponding simulated tracks denoted by *B* and *C*, respectively. The best track is plotted by a *black curve*

of the cyclone in the lower troposphere. Assimilation of GPS RO soundings produces dryness at lower levels and cooling in the upper troposphere. The GPS sensitivity experiments that assimilate only some of the GPS RO soundings show that the simulated tracks are more sensitive to the RO soundings in the vicinity of the cyclone. The simulated track is not improved when only the RO information above 14 km is retained. These experiments highlight the importance of upper tropospheric RO information in driving the cyclone. The GPS RO retrieved dry temperature is known to possess high accuracy in upper troposphere and lower stratosphere (UTLS) (Anthes et al. 2008). In this study, we found the positive impact of the GPS data on cyclone track prediction due to contributions from assimilation of their accurate temperature in the upper troposphere. It has been well known that the GPS RO retrieved refractivity may contain negative biases in the lower

troposphere (Kuo et al. 2004; Poli et al. 2010; Anthes 2011). Therefore, the low-level information of RO data may be discarded while keeping their upper-level information, when biases are unavoidable in the retrieved refractivity at lower levels due to super-refraction conditions (e.g., Kuo et al. 2004; Sokolovskiy et al. 2003).

Further, we also compare the results of GPS assimilation experiment with GTS data assimilation. The relative advantages of the data impacts are discussed in this study. Overall, GPS performs best in terms of track prediction with a reduced cross-track error at later stages. To understand the track improvement at later stages (72–96 h) for GPS, we investigated the difference of moisture and sea-level pressure between GPS and CTL. It is noticed that a couplet was induced with low pressure and moist air to the left and high pressure and dry air to the right. This couplet pattern became stronger from 48 to 60 h. The horizontal pressure gradient force might be the reason for why the GPS track is driven closer to the best track at the later stage. For cyclone intensity prediction, GPS-cyc experiment outperforms the others due to use of more soundings. Owing to the high vertical resolution of RO soundings and high accuracy in retrieved temperature in UTLS, the RO soundings may help to better resolve the synoptic steering flow condition where the storm is embedded.

The impacts of GPS RO data in tropical cyclone prediction emerge through complicated nonlinear processes and are only partially illustrated or explained by initial and forecast difference analyses of specifically designed sensitivity experiments. We realize that any small tiny difference may likely result in significant forecast errors when tropical cyclone evolution is sensitive to some observation impact region. Furthermore, nonlinear advective and diffusive processes can mix up with microphysical processes, and in a long run, positive or negative impacts depend on how the cyclone is in response to the evolving processes. Thus, the combination of different sets of observations may not necessarily give further positive impacts even any of which does have a positive or neutral impact (Huang et al. 2010). In this study, we identify the mechanism that why the track can be driven dynamically due to positive impacts of observations.

In a prospective view, the impact of the GPS RO soundings on track prediction of a super cyclone, as shown in this study, encourages application of RO data to severe weather prediction. Optimistically, we may expect that more RO data in higher horizontal density should lead to larger impacts on cyclone prediction. The FORMOSAT-3/COSMIC follow-on mission (COSMIC-2) will start with a first launch of 6 LEOs in early 2016, followed by the second launch of 6 LEOs in 2018, to track signals from GPS and GALILEO and GLONASS (a Tri-G constellation network), and will provide daily RO data about four times the average amount ($\sim 2,000$) from the FORMOSAT-3/COSMIC constellation. We are looking forward to exploring forecast impacts of plentiful RO data from such a future mission.

Acknowledgments This work is supported by National Science Council and National Space Organization in Taiwan.

References

- Anthes RA (2011) Exploring Earth's atmosphere with radio occultation: contributions to weather, climate and space weather. *Atmos Meas Tech* 4:1077–1103
- Anthes RA et al (2008) The COSMIC/FORMOSAT-3 mission: early results. *Bull Am Meteorol Soc* 89:313–333

- Barker DM, Huang W, Guo Y-R, Bourgeois AJ, Xiao QN (2004) A three-dimensional variational data assimilation system for MM5: implementation and initial results. *Mon Weather Rev* 132:897–914
- Chen S-Y, Huang C-Y, Kuo Y-H, Guo Y-R, Sokolovskiy S (2009) Assimilation of GPS refractivity from FORMOSAT-3/COSMIC using a nonlocal operator with WRF 3DVAR and its impact on the prediction of a typhoon event. *Terr Atmos Oceanic Sci* 20:133–154
- Chen S-Y, Huang C-Y, Kuo Y-H, Sokolovskiy S (2011) Observational error estimation of GPS radio occultation refractivity and excess phase data. *Mon Weather Rev* 139:853–865
- Cucurull L (2010) Improvement in the use of an operational constellation of GPS radio occultation receivers in weather forecasting. *Weather Forecast* 25:749–767
- Cucurull L, Kuo Y-H, Barker D, Rizvi SRH (2006) Assessing the impact of simulated COSMIC GPS radio occultation data on weather analysis over the Antarctic: a case study. *Mon Weather Rev* 134:3283–3296
- Healy SB (2008) Forecast impact experiment with a constellation of GPS radio occultation receivers. *Atmos Sci Lett* 9:111–118
- Healy SB, Thepaut J-N (2006) Assimilation experiments with CHAMP GPS radio occultation measurements. *Q J R Meteorol Soc* 132:605–623
- Healy SB, Jupp AM, Marquardt C (2005) Forecast impact experiment with GPS radio occultation measurements. *Geophys Res Lett* 32:L03804
- Huang C-Y, Kuo Y-H, Chen S-H, Vandenberghe F (2005) Improvements on typhoon forecast with assimilated GPS occultation refractivity. *Weather Forecast* 20:931–953
- Huang C-Y, Kuo Y-H, Chen S-Y, Rao ASKAVP, Wang C-J (2007) The assimilation of GPS radio occultation data and its impact on rainfall prediction along the west coast of India during monsoon 2002. *Pure Appl Geophys* 164:1577–1591
- Huang C-Y, Kuo Y-H, Chen S-Y, Terng C-T, Chien F-C, Lin P-L, Kueh M-T, Chen S-H, Yang M-J, Wang C-J, Rao ASKAVP (2010) Impact of GPS radio occultation data assimilation on regional weather predictions. *GPS Solut* 14:35–49
- Kliore AJ, Hamilton TW, Cain DL (1964) Determination of some physical properties of the atmosphere of Mars from changes in the Doppler signal of a spacecraft on an earth occultation trajectory. Jet Propulsion Laboratory, Technical Report, Pasadena, CA, pp 32–674
- Krishnamurti TN, Bedi HS, Ingles K (1993) Physical initialization using SSM/I rain rates. *Tellus* 45A:247–269
- Krishnamurti TN, Bhowmik SKR, Oosterhof D, Rohaly G (1995) Mesoscale signatures within the Tropics generated by physical initialization. *Mon Weather Rev* 123:2771–2790
- Kueh M-T, Huang C-Y, Chen S-Y, Chen S-H, Wang C-J (2009) Impact of GPS radio occultation soundings on prediction of Typhoon Bilis 2006 landfalling Taiwan. *Terr Atmos Ocean Sci* 20:115–131
- Kuo Y-H, Zou X, Huang W (1997) The impact of GPS data on the prediction of an extratropical cyclone: an observing system simulation experiment. *J Dyn Atmos Ocean* 27:413–439
- Kuo Y-H, Sokolovskiy S, Anthes RA, Vandenberghe F (2000) Assimilation of GPS radio occultation data for numerical weather prediction. *Terr Atmos Ocean Sci* 11:157–186
- Kuo Y-H, Wee T-K, Sokolovskiy S, Rocken C, Schreiner W, Hunt D, Anthes RA (2004) Inversion and error estimation of GPS radio occultation data. *J Meteorol Soc Jpn* 82:507–531
- Kursinski E, Hajj G, Schofield J, Linfield R, Hardy K (1997) Observing earth's atmosphere with radio occultation measurements using the Global Positioning System. *J Geophys Res* 102:23429–23465
- Kursinski ER, Hajj GA, Leroy SS, Herman B (2000) The GPS radio occultation technique. *Terr Atmos Ocean Sci* 11:53–114
- Liu H, Zou X (2003) Improvements to GPS radio occultation ray-tracing model and their impacts on assimilation of bending angle. *J Geophys Res* 108(D17):4548. doi:10.1029/2002JD003160
- Liu H, Anderson J, Kuo Y-H, Snyder C, Caya A (2008) Evaluation of a nonlocal quasi-phase observation operator in assimilation of CHAMP radio occultation refractivity with WRF. *Mon Weather Rev* 136:242–256
- Ma Z, Kuo Y-H, Wang B, Wu W-S, Sokolovskiy S (2009) Comparison of local and non-local observation operators for the assimilation of GPS radio occultation refractivity data in the NCEP GSI system: an observing system simulation experiment. *Mon Weather Rev* 137:3575–3587
- Poli P, Moll P, Puech D, Rabier F, Healy SB (2008) Quality control, error analysis, and impact assessment of FORMOSAT-3/COSMIC in numerical weather prediction. *Terr Atmos Ocean Sci* 20:101–113
- Poli P, Healy SB, Dee DP (2010) Assimilation of Global Positioning System radio occultation data in the ECMWF ERA–Interim reanalysis. *J R Meteorol Soc* 136:1972–1990
- Potty J, Oo SM, Raju PVS, Mohanty UC (2012) Performance of nested WRF model in typhoon simulations over West pacific and South China Sea. *Nat Hazard* 63(3):1451–1470

- Raju PVS, Potty J, Mohanty UC (2011) Sensitivity of physical parameterizations on prediction of tropical cyclone Nargis over the Bay of Bengal using WRF model. *Meteorol Atmos Phys*. doi:[10.1007/s00703-011-0151-y](https://doi.org/10.1007/s00703-011-0151-y)
- Sokolovskiy S, Kuo Y-H, Rocken C, Schreiner WS, Hunt D, Anthes RA (2003) Effect of superrefraction on inversions of radio occultation signals in the lower troposphere. *Radio Sci* 38:1058. doi:[10.1029/2002RS002728](https://doi.org/10.1029/2002RS002728)
- Sokolovskiy S, Kuo YH, Wang W (2005a) Assessing the accuracy of linearized observation operator for assimilation of the Abel-retrieved refractivity: case simulation with high-resolution weather model. *Mon Weather Rev* 133:2200–2212
- Sokolovskiy S, Kuo YH, Wang W (2005b) Evaluation of a linear phase observation operator with CHAMP radio occultation data and high-resolution regional analysis. *Mon Weather Rev* 133:3053–3059
- Zou X, Vandenberghe F, Wang B, Gorbunov ME, Kuo Y-H, Sokolovskiy S, Chang JC, Sela JG, Anthes R (1999) A raytracing operator and its adjoint for the use of GPS/MET refraction angle measurements. *J Geophys Res* 104:22301–22318
- Zou X, Wang B, Liu H, Anthes RA, Matsumura T, Zhu YJ (2000) Use of GPS/MET refraction angles in 3D variational analysis. *Q J R Meteorol Soc* 126:3013–3040